1967-09

Mass conservative attitude control systems for interplanetary spacecraft.

Gilbreath, David Slagle

Monterey, California. U.S. Naval Postgraduate School

MASS CONSERVATIVE ATTITUDE CONTROL SYSTEMS FOR INER-PLANETARY SPACECRAFT

DAVID SLAGLE GILBREATH

TABLE OF CONTENTS

LIST OF FIGURES

SYMBOLS

A	-	Angular impulse, ft-lb-sec
D	-	Damping torque per unit relative angular speed, ft-lb-sec/rad
E	-	Energy, ft-lb
$\bar{H}$	-	Angular momentum about center of mass, ft-lb-sec
I	-	Mass moment of inertia, ft-lb-sec^2
P	-	Power, watts
S	-	Absolute angular speed of ACS spin axis, rad/sec
T	-	Torque, ft-lb
t	-	Time, sec
X	-	Vector cross product operator
ω	-	Vehicle absolute angular speed, rad/sec
Ω	-	Angular speed of ACS rotating element relative to vehicle, rad/sec
$\bar{i}, \bar{j}, \bar{k}$	-	Unit vectors along vehicle x, y and z principal axes, respectively

NOTATION

Letters with overbars are vector quantities. Unbarred quantities are scalar. A dot over a quantity denotes the time derivative of that quantity.

TERMINOLOGY AND ABBREVIATIONS

ACS - Attitude control system/systems

DOF - Degree/degrees of freedom

CMG - Control moment gyro/gyros

ME - Momentum exchange

SYSTEM - Denotes the entire spacecraft

VEHICLE - That part of the system separate from a smaller rotating component of the system

SUBSCRIPTS

c - Control; e.g., T_c, control torque

D - Disturbance; e.g., T_D, disturbance torque

M - Torque motor; e.g., T_M, torque motor torque

R - About the spin axis of the rotating element; e.g., H_R, angular momentum of ACS about the spin axis

v - Vehicle; e.g., H_v, angular momentum of vehicle

x,y,z - Vehicle principal axis; e.g., T_x, control torque about the x axis

SECTION I

INTRODUCTION

Future space travel will involve substantial increases in vehicle size and trip length. Flight paths presently under consideration are low thrust, minimum energy trajectories with long free fall stages. A typical proposed round trip is the Mars flyby which requires about 700 days. It is for such long duration flights that the attitude control systems (ACS) discussed in this paper might be employed. Torque producing jet thrusters have been utilized in all manned space flights to date and are optimum for short duration flights. For the longer voyages contemplated, the amount of fuel required for attitude control thrusters becomes an appreciable percentage of total system weight and storage space. It is this factor that has prompted the search for a substitute for mass expulsion ACS.

The mass conservative ACS considered in this thesis are described in Sec. III and compared in Sec. IV. Immediately following is a discussion of attitude control requirements.

SECTION II

ATTITUDE CONTROL REQUIREMENTS

Need for attitude control may arise from the following:

1. Vehicle orientation for use of main thrust engines, solar cells, navigation and communication equipment, etc.
2. Docking
3. Crew and component limitations on vehicle angular velocity.

Orientation for scientific measurements may well be the most demanding in terms of frequency and accuracy. Interplanetary trajectories usually involve midcourse guidance; some programs require several velocity changes with corresponding demands on navigational information. The ability of data gathering instruments to compensate for vehicle attitude error is often quite limited; the Orbiting Astronomical Laboratory concept allows a vehicle pointing error of 0.1 arc second. Torque magnitudes are mentioned later in this report.

Control torque serves to give the vehicle the desired angular velocity and orientation and to counter disturbance or unwanted torque. Disturbance torques are conveniently categorized by origin as follows.

Internally caused torque. Interaction between components of a spacecraft system does not affect the total angular momentum of the system, but it can change the angular motion of the vehicle; e.g., the stopping or starting of a rotary pump does not change the angular momentum of the system but it does torque the vehicle. Gyroscopic torque results from precession of the momentum of rotating machinery. Sources of these torques include tape recorders and motion of antennas, crew and stored liquid. For the Apollo vehicle, 100 seconds of arc per second represents a typical disturbance from crew movement. [1]

Externally caused disturbance torque. Sources of external disturbance torque are:

1. Gravity gradient
2. Solar radiation pressure
3. Magnetic field
4. Micrometeorite impingement
5. Thermal radiation from vehicle
6. Gas leaks, outgassing of vehicle material
7. Unwanted torque from ACS
8. Unwanted torque from main thrust engines

The facing of the same side of the moon toward earth is due to gravity gradient torque. The salient features of this torque are described in Appendix A. As well as being dependent on system orientation and mass distribution, gravity gradient torque decreases rapidly with increasing distance between bodies. The importance of gravity gradient as a disturbance or control torque gives way to solar radiation pressure at about 600 miles from earth. Therefore, although gravity gradient has been successfully employed for earth satellite stabilization, it is of little concern for interplanetary travel.

Discussion of solar radiation torque is given in Sec. III.

Like gravity gradient, magnetically induced torque is important only in the near vicinity of earth or other bodies with surrounding magnetic fields.

Quantitative assessment of micrometeorite induced torque will remain difficult until more data are accumulated on the sizes, velocities and distribution of these particles. Although the sizes and collision frequency are expected to be low, the engaging speeds are such as to

impart considerable momentum to a spacecraft. The extent to which meteorites produce unbalanced torque is, of course, a function of vehicle geometry. Protruding solar energy collectors and antennas render spacecraft more susceptible to this torque.

Inefficiencies in spacecraft energy conversion devices necessitate thermal radiation from the vehicle. The torque produced by thermal radiation is minor and readily design controlled.

Gas leaks and outgassing of vehicle surface material would normally cause very small torques.

ACS non-zero pointing error results from imperfect attitude sensors and/or control systems which cause oscillations or limit cycles about the desired orientation. Momentum exchange (ME) ACS produce unwanted torque due to gyroscopic coupling; this phenomenon is discussed later.

During powered flight, directional control of the main engine thrust vector by nozzle gimballing, or other means, affords two axis attitude control; however, supplemental attitude control may be necessary to meet accuracy requirements.

Dynamic requirements of ACS. For a given system, pointing accuracy and response time constitute the dynamic capability of the ACS. Since response time is a function of control torque, the latter parameter, being more convenient and general, is used for comparison purposes.

The governing general equation of angular motion for a system of masses reduces to simplified equations in limiting cases. The derivation and listing of these equations, Nos. 1-9, are in Appendix B. These equations appear in this paper without lengthy explanation and bear the same identifying number as given in Appendix B. Equation (10) and subsequent equations are developed in context. An assumption made throughout is

that, in response to control or disturbance torque, the vehicle behaves as a rigid inelastic body; i.e., the effect on vehicle motion of component interactions is neglected. These interactions are accompanied by transfer of kinetic to thermal energy and must be considered when dealing with spin stabilized vehicles. Spin stabilization is an unlikely choice for interplanetary flight due to the need for fixed orientation for the use of solar energy collectors, antennas and other apparatus.

The dynamics of rigid body angular motion is described by the following equation.

$$\bar{T} = \left[I_{xx}\dot{\omega}_x + (I_{zz} - I_{yy})\omega_y\omega_z\right]\bar{i} + \left[I_{yy}\dot{\omega}_y + (I_{xx} - I_{zz})\omega_x\omega_z\right]\bar{j} + \left[I_{zz}\dot{\omega}_z + (I_{yy} - I_{xx})\omega_x\omega_y\right]\bar{k} \quad , \tag{3}$$

where: $\bar{T}$ = sum of control and disturbance torques

I = mass moment of inertia

ω = vehicle angular speed

The coordinate system is fixed in the vehicle and aligned with the vehicle's principal axes. The kinematical equations relating angular displacement, velocity and acceleration and response time require a coordinate transformation to Eulerian Angles or their equivalent. For the purposes of this thesis it suffices to note that response time is a function of acceleration, and this acceleration is torque generated as indicated in Eq. (3).

SECTION III

ATTITUDE CONTROL SYSTEMS

ACS may be termed passive if they do not require energy or mass expenditure. In the active category are jet thrusters and momentum exchange devices. Passive control torque is obtained from some of the same environmental sources that cause external disturbance torque; namely, gravity gradient, magnetic field and solar radiation. For reasons previously set forth, only the last of these is significant for interplanetary travel. Solar radiation is also spatially variant but not so unfavorably, as indicated in Fig. 1.

Solar radiation torque. Although not the only electromagnetic radiation in our solar system, the sun's emissions dwarf those of all others combined and need be the only radiation considered. Incident radiation is either absorbed or reflected, the reflected part being diffuse or specular. Figure 2 illustrates the three possibilities. The radiation force on a surface is the time derivative of the incident momentum. Using Einstein's mass energy equivalency:

$$\bar{F} = \frac{d(m\bar{c})}{dt} = \frac{d}{dt}\left(\frac{\bar{E}}{c}\right) ,$$

where E is the incident energy and c is the speed of light. With P_f defined as the pressure of fully absorbed radiation perpendicular to the surface, the expression for solar pressure is:

$$\bar{P} = \left[\frac{2}{3}\rho(1-s)\cos\theta + (1+s\rho)\cos^2\theta\right] P_f \bar{N} + (1-s\rho) P_f \cos\theta \sin\theta \bar{t} ,$$

where θ and the unit vectors $\bar{N}$ and $\bar{t}$ are shown in Fig. 2. The symbols ρ and S are defined as follows:

$0 < \rho < 1$ = fraction of incident radiation reflected

$0 < S < 1$ = fraction of reflected radiation reflected specularly

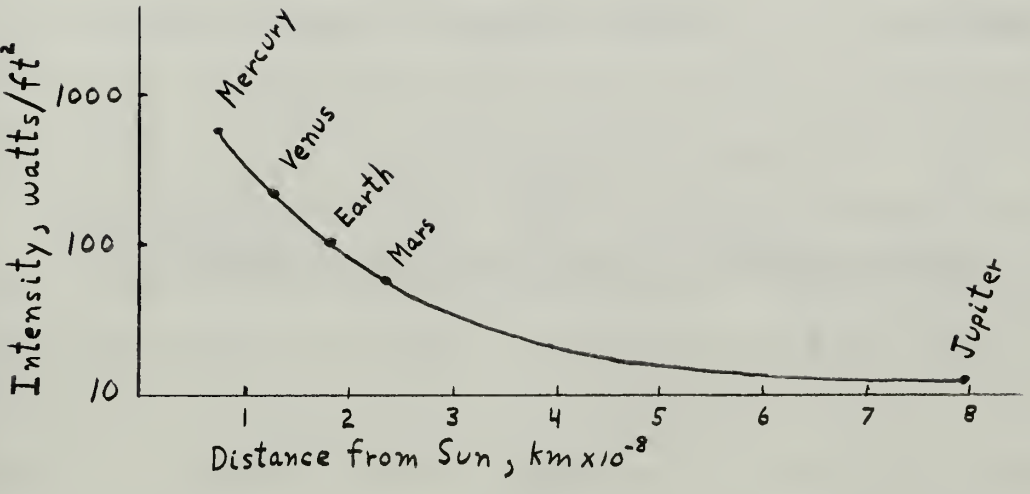

Figure 1

Sun's Radiation versus Distance from the Sun

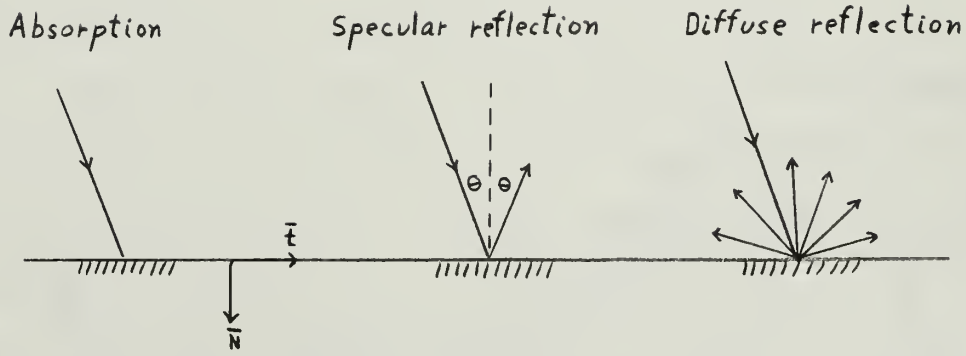

Figure 2

Radiation Absorption and Reflection

If $\theta = 0$ and $\rho = S=1$, the maximum pressure of 2 P_f is realized. At an earth's distance from the sun $P_f = 9.8 \times 10^{-8}$ lb/ft^2.

Torque generated by solar pressure will, of course, be dependent on moment arm and control surface area as well as the parameters in the pressure equation. The following example illustrates the order of magnitude of solar torque. A non-absorbing, specularly reflecting panel, 10 ft by 10 ft, with a moment arm of 10 ft and oriented normal to the sun's radiation at an earth's distance from the sun, will exert a torque of 19.6×10^{-5} ft-lb. Figure 3 shows some conceptual designs that have appeared in the literature; Figs. 3(b) and 3(c) are self aligning energy collectors. It seems likely that if solar torque is utilized for attitude control, it will be in the form of such dual purpose devices.

Active ACS. Active ACS are mass expulsion and momentum exchange (ME) devices. In the latter group are reaction wheels, reaction spheres and control moment gyros (CMG). The three ME ACS provide torque by changing the angular momentum of a mass within the vehicle. Their torque is "internal"; therefore, any change in system angular momentum is due to external disturbance torque. The first two devices effect momentum exchange between vehicle and ACS by changing the angular speed of a wheel or sphere. The CMG maintains constant angular speed and effects momentum exchange by altering the direction of the rotating element's spin axis. In equation form the ME ACS are described by:

Reaction wheel or sphere:

$$\bar{T}_c = -\left[\frac{d\bar{H}_R}{dt}\right]_{\bar{S}=0} = -I_R \left[\frac{d(\bar{\Omega}+\bar{\omega}_R)}{dt}\right]_{\bar{S}=0} \tag{8}$$

CMG: $$\bar{T}_c = -\bar{S} \times \bar{H}_R = -I_R(\bar{S} \times \bar{\Omega}) \quad , \tag{9}$$

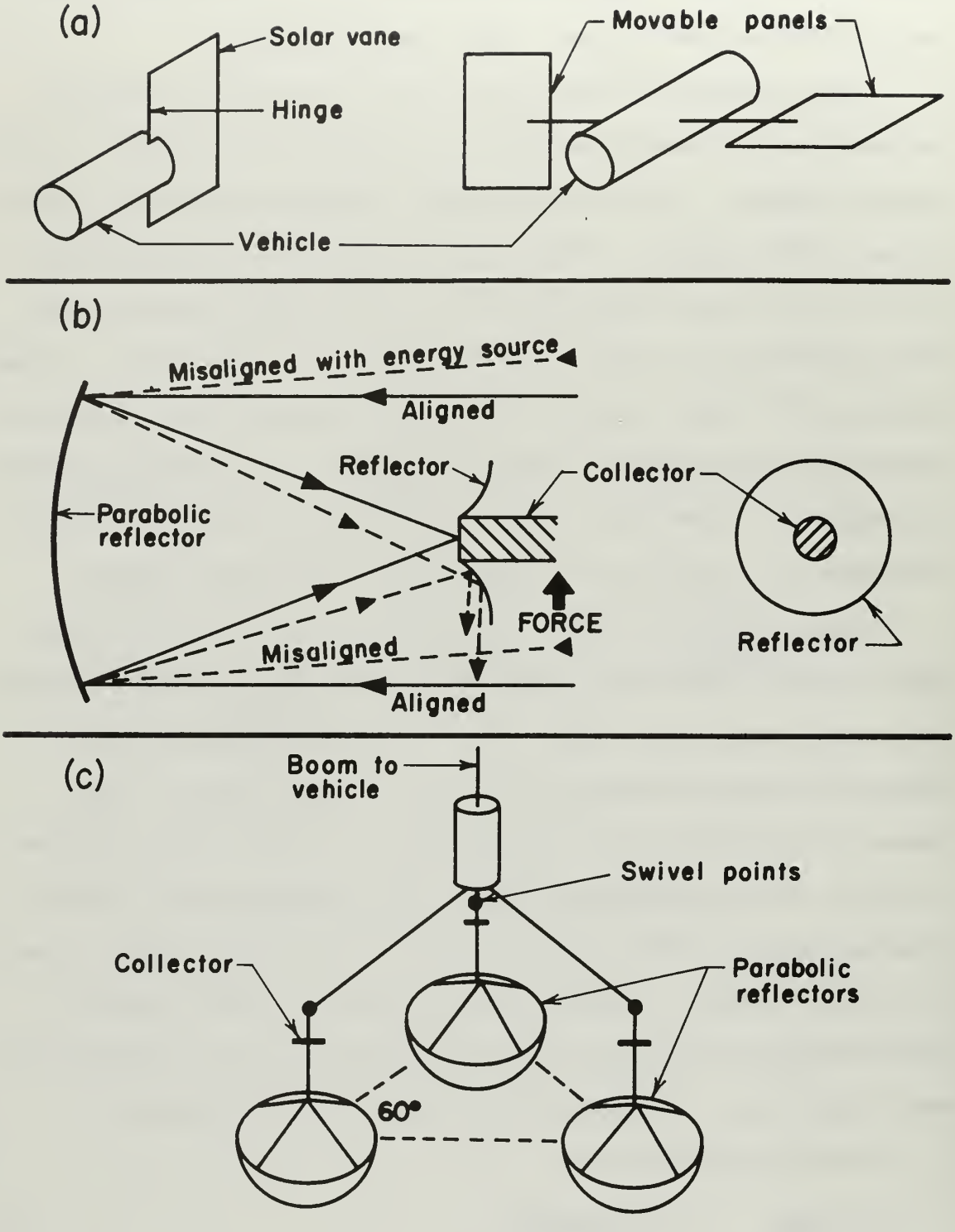

Figure 3

Solar Torquers and Energy Collectors

where: $\bar{T}_c$ = control torque

$\bar{H}_R$ = ACS angular momentum

$\bar{S}$ = absolute angular velocity of the ACS spin axis

$\bar{\Omega}$ = angular speed of the wheel or sphere relative to the vehicle

$\bar{\omega}_R$ = component of vehicle angular velocity about the ACS spin axis

A more detailed description of the three basic ME ACS follows.

Reaction wheel. A reaction wheel is a motor driven wheel. The motor exerts a control torque on the vehicle and an equal and opposite torque on the wheel. The torque axis is fixed with respect to the vehicle. Three such wheels with mutually perpendicular spin axes provide complete attitude control; normally the spin axes would be parallel to vehicle principal axes to reduce the coupling evident in Eq. (3).

For a reaction wheel parallel to the vehicle x axis, combining Eqs. (3) and (8) yields:

$$T_c = I_R(\dot{\Omega} - \dot{\omega}_x) = T_D + I_{xx}\dot{\omega}_x + (I_{zz} - I_{yy})\omega_y\omega_z \quad , \tag{10}$$

where T_D is disturbance torque, and the assumption is made that the moments of inertia of the vehicle approximate those of the system. For the case of steady pointing Eq. (10) reduces to:

$$T_c = I_R\dot{\Omega} = T_D \tag{11}$$

For attitude changes in interplanetary space, the control torque required for reasonable response time is normally much greater than disturbance torque, a possible exception being the disturbance torque resulting from misalignment of the main engine thrust vector. With this assumption, Eq. (10) becomes, for the case of commanded reorientation:

$$T_c = I_R(\dot{\Omega} - \dot{\omega}_x) = I_{xx}\dot{\omega}_x + (I_{zz} - I_{yy})\omega_y\omega_z \tag{12}$$

Power required, less motor, bearing and windage losses, is, using Eq. (10):

$$P = T_c\,\Omega = I_R(\dot{\Omega} - \dot{\omega}_x)\Omega \tag{13}$$

Energy required, less the losses previously noted, is, using Eqs. (10) and (13):

$$E = \int_1^2 P\,dt = I_R\int_1^2(\dot{\Omega} - \dot{\omega}_x)\Omega\,dt = I_R\int_1^2(\dot{\Omega} - \dot{\omega}_x)(\Omega - \omega_x)\,dt + I_R\int_1^2(\dot{\Omega} - \dot{\omega}_x)\omega_x\,dt = \frac{I_R}{2}\left[(\Omega_2 - \omega_{x_2})^2 - (\Omega_1 - \omega_{x_1})^2\right] + \int_1^2 T_c\,\omega_x\,dt \tag{14}$$

The maximum angular impulse absorbed by the wheel, assuming the wheel initially at rest and using Eq. (10), is:

$$A_{max} = \int T_c\,dt = I_R\int(\dot{\Omega} - \dot{\omega}_x)\,dt \simeq I_R\,\Omega_{max}\quad , \tag{15}$$

where the assumption is made that $\Omega_{max} \gg \omega_x$.

Optimization of any ME ACS consists of arriving at the proper blend of the following objectives, commensurate with cost and reliability specifications:

1. Maximize control torque
2. Maximize angular impulse capacity
3. Minimize power and energy
4. Minimize weight
5. Minimize space

With respect to a reaction wheel the following points evolve:

1. Objective 4 and the need for large wheel moment of inertia dictate a wheel with its mass concentrated in the rim.
2. Objectives 3 and 4 are in direct conflict with one another;

for a given control torque, decreasing I_R necessitates a higher wheel angular acceleration with resulting increase in power and energy. Reference [2] accounts for this compromise by minimizing an "equivalent weight" which is a function of power as well as weight. This function is a measure of the relative importance of power and weight and is representative of the need for a systems approach to ACS selection and design.

The equations that have been derived for a reaction wheel are for a single wheel. The three wheels required for three axis control would, in general, all be spinning. Precession of this momentum by vehicle angular velocity results in gyroscopic torque. The torque, then, for a set of reaction wheels is, according to Eq. (6):

$$\bar{T}_c = -\left[\frac{d\bar{H}_R}{dt}\right]_{\bar{S}=0} - \bar{S} \times \bar{H}_R \quad , \tag{6}$$

where, in this case, $\bar{H}_R$ is the net momentum of the three wheels and $\bar{S} = \bar{\omega}$. Normally the first term would be predominant. The second term in Eq. (6) is, in general, unwanted since it increases the power required for attitude changes; however, it does afford rate damping for steady pointing. Damping serves to reduce oscillations or limit cycling caused by electromechanical lag in the motor-wheel-vehicle combination. Eddy current, viscous and hysteresis damping have been suggested. Reference [3] claims weight and size advantages for the hysteresis damper. Their design weighs one pound, provides 1.5 ft-lb per rad/sec and consists of permanent magnets attached to the controller housing on either side of a thin vane protruding from the wheel rim. Damping torque results from local magnetization polarity changes in the vane material

as it moves relative to the magnets. Appendix C is a brief description of a reaction wheel built for NASA.

Reaction sphere. The reaction sphere has the singular capability, among ME devices, of providing torque about any axis. Due to weight and moment of inertia considerations it takes the form of a spherical shell. Lacking mechanical supports it may be suspended by gas bearings, a magnetic field, or an electric field. Gas bearing suspension causes high viscous losses and limited positioning force. If the sphere has equal moments of inertia and the torquing imparts no radial forces, positioning force is necessary only to counter vehicle linear accelerations and centrifugal forces due to vehicle angular speed. Reference [4] suggests magnetic suspension in the form of three orthogonal pairs of servo controlled electromagnets surrounding the sphere. Positioning force results from interaction between the applied magnetic field and eddy currents induced in the spherical shell. Some drag torque results from this type of suspension. Electric field suspension is the only means that does not cause drag torque on the sphere; however, positioning force is restricted by the limited voltage gradient maintainable between housing and sphere.

Torquing the sphere magnetically has been proposed. Reference [5] suggests an electrostatically suspended, electromagnetically torqued sphere as pictured in Fig. 4. As with magnetic suspension, torque results from interaction between the applied field and eddy currents induced in windings in the sphere's shell. In this design there are three orthogonal stator windings in the shell. The magnetic field rotates, "dragging" along the sphere. Eight electrode areas on the shell and four pairs of electrodes in the housing afford four independent

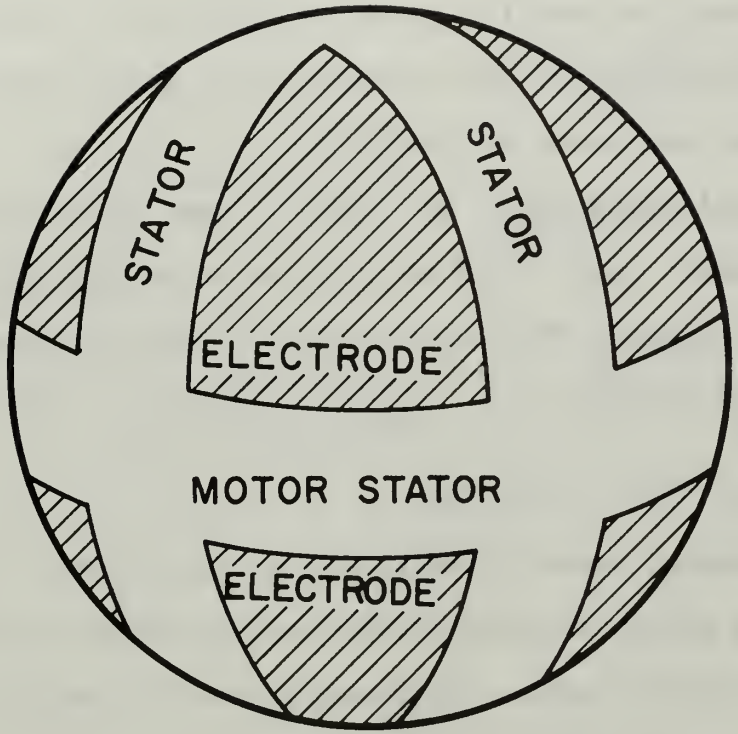

Figure 4

Electrostatically Supported Magnetically

Torqued Reaction Sphere

positioning forces. The electrodes ideally cover the sphere surface except for motor stators.

If a reaction sphere is magnetically torqued and suspended, there is unwanted interaction between the magnetic fields. Reference [4] recommends such an arrangement with the claim that this interaction is negligible. A description of this device is in Appendix D.

Although the reaction sphere has theoretical advantages, it has not reached the hardware stage because of large scale problems associated with sphere suspension and torquing.

Control moment gyro. The final and most promising ME ACS is the control moment gyro. A CMG may have one or two degrees of freedom; both will be discussed. The device produces torque by precessing the angular momentum of a wheel.

$$\bar{T}_c = -\bar{S} \times \bar{H}_R = -I_R(\bar{S} \times \bar{\Omega}) \tag{9}$$

$\bar{S}$, the absolute angular velocity of the CMG spin axis, is the vector sum of vehicle angular velocity and the angular velocity of the spin axis relative to the vehicle. The latter motion is effected by a torque motor as shown in Fig. 5.

The angular speed of the wheel is held constant by a drive motor which, aside from initial speed buildup, needs to overcome only bearing and windage losses. In Fig. 5 the torque motor torque, T_M, acts on the gimbal; an opposite and equal torque acts on the vehicle. This convention will be followed in subsequent figures. The damper represents natural and artificial damping. S_2 is the component of vehicle angular speed about the output axis; S_1 is the gimbal angular speed. For the angular directions assumed in Fig. 5, the gimbal equation of motion is:

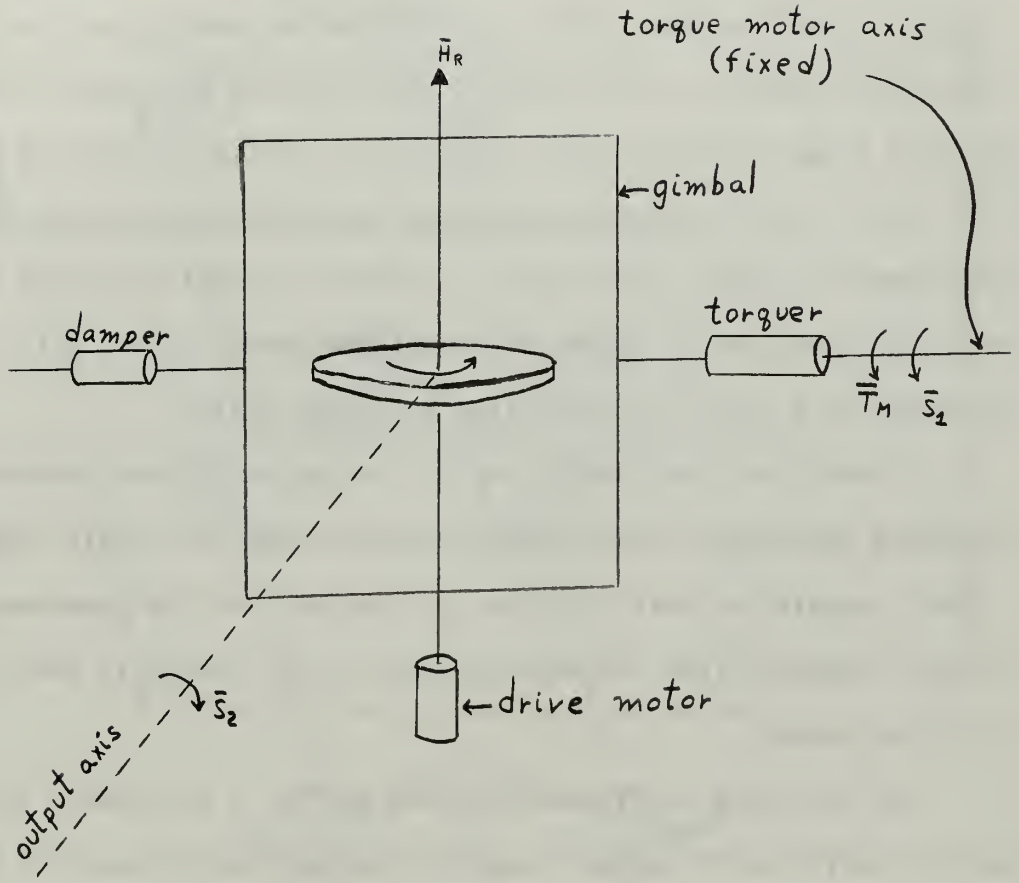

Figure 5

Single Degree of Freedom Control Moment Gyro

$$T_M - D\dot{\theta} + S_2 H_R = I\dot{S}_1 \quad , \tag{16}$$

where I is the moment of inertia of the gimbal and rotor about the torque motor axis. $S_2 H_R$ is a gyroscopic torque. $D\dot{\theta}$ is the damping torque, where $\dot{\theta}$ is the gimbal angular speed relative to the vehicle. Unwanted torques on the vehicle are those of the damper and the torque and drive motors; normally these would be much less than the output torque $S_1 H_R$. A more serious problem arises from the output axis not remaining fixed with respect to the vehicle. As mentioned previously it is desirable to align the output axis parallel to a vehicle principal axis; the CMG output axis remains perpendicular to the fixed torque motor axis and the wheel spin axis. Therefore, to minimize coupling, such a device must be restricted to small gimbal displacements. Three axis control is provided by a CMG for each vehicle principal axis.

As with reaction wheels, such a configuration must contend with unwanted gyroscopic torque due to precession of the wheels' momenta by vehicle angular velocity. Since, in general, the CMG possesses a higher angular momentum than the reaction wheel, the problem is more severe with the former.

The twin gyro configuration shown in Fig. 6 provides a fixed output axis relative to the vehicle and substantially alleviates the problem of the preceding paragraph. The three axes shown in Fig. 6 are orthogonal. Not shown are the two drive motors that maintain the two wheels at a constant and equal speed. The torquers are coordinated so that both wheels are precessed an equal amount at the same rate. The neutral positions of the angular momentum vectors are along the spin reference axis pointing inward.

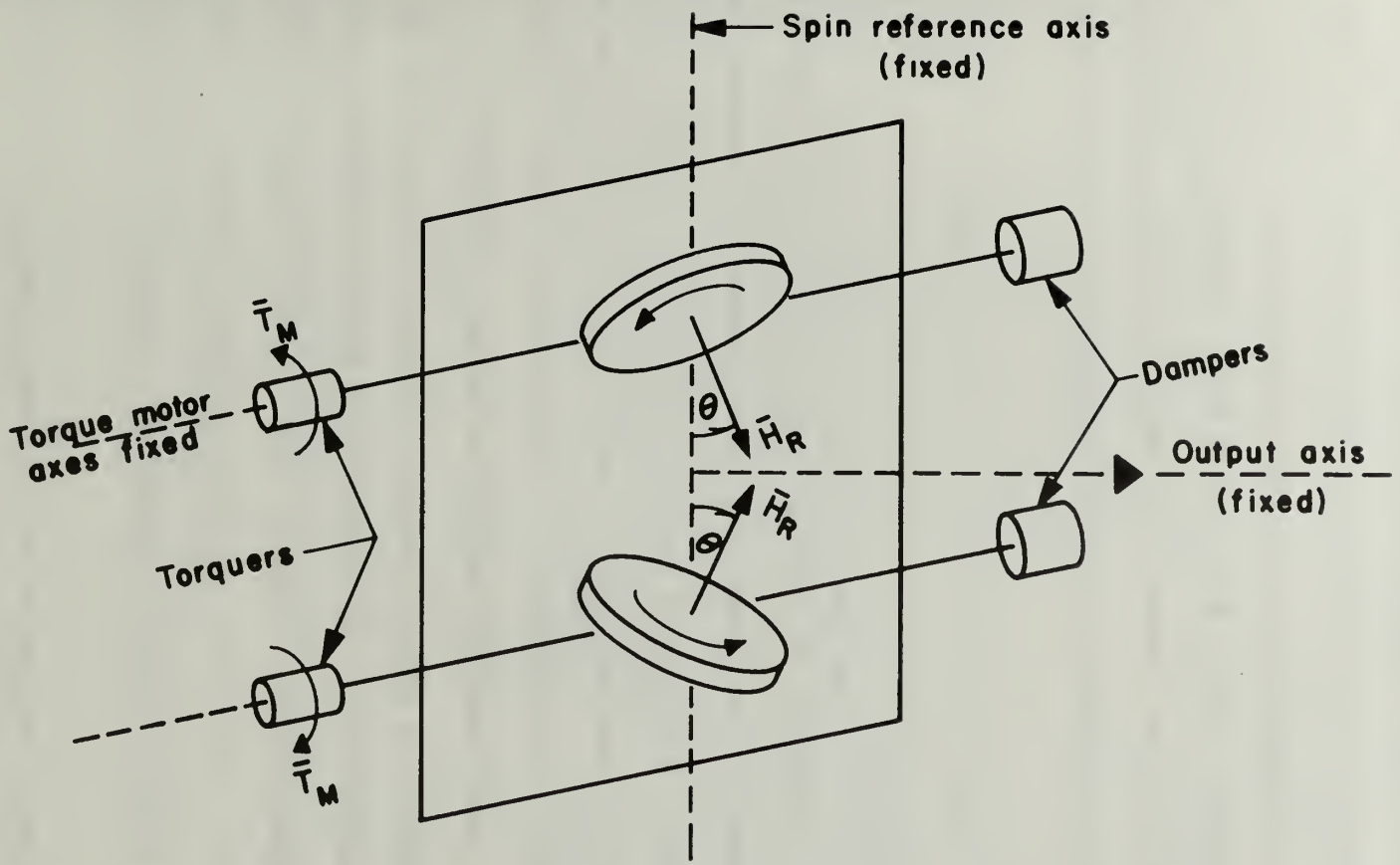

Figure 6

Twin Single Degree of Freedom Control Moment Gyro

The absolute angular rate about the torque motor axis of each spin axis is the sum of its angular speed relative to the vehicle, $\dot{\theta}$, and the component of vehicle angular speed about the torque motor axis. For this configuration it is convenient to consider separately the gyroscopic torque effected by each of these angular rates.

The gyroscopic torque, $\dot{\theta} H_R$, is of equal magnitude for both wheels. The components of these torques along the spin reference axis are equal and opposite; the components along the output axis are additive and together equal:

$$T_c = 2 H_R \dot{\theta} \cos\theta \qquad (17)$$

The reactance torques on the vehicle from the torquers and dampers are equal and opposite, thus eliminating a minor source of unwanted torque. The output axis is permanently parallel to a vehicle principal axis. With the twin gyro configuration the wheel momenta cancel to some extent; the net momentum is $2H_R \sin\theta$ and is directed along the output axis. Vehicle angular speed about the spin reference and torque motor axes acts on the net momentum to produce unwanted gyroscopic torque about the other axis, respectively. An increase in θ has two detrimental effects: The net momentum increases, causing larger coupling torques, and control torque, Eq. (17), decreases. Therefore a gimbal limit prior to the $\theta = 90^{\circ}$ zero torque position is suggested; reference [1] limited θ to $\pm 60^{\circ}$.

The equation of motion for an individual gimbal is comparable to Eq. (16). The output axis is again assumed parallel to the vehicle x axis.

$$T_M - D\dot{\theta} - \omega_x H_R \cos\theta - \omega_y H_R \sin\theta \simeq I\ddot{\theta} \qquad (18)$$

where the signs of the third and fourth terms are dependent on the directions of ω_x and ω_y, respectively, and the relative angular acceleration, $\ddot{\theta}$, approximates the absolute gimbal angular acceleration. The other quantities are the same as in Eq. (16). If the suggested gimbal limits are observed, Eq. (18) can be closely approximated by:

$T_M \simeq I\ddot{\theta} + \omega_x H_R \cos\theta$. Power required, less motor losses, for both torquers is:

$$P = 2T_M \dot{\theta} = 2(I\ddot{\theta} + \omega_x H_R \cos\theta)\dot{\theta} \tag{19}$$

As with the single CMG, drive motor torque for constant speed operation is necessary only to counter bearing and windage torques. To preclude unnecessarily large drive motors, a long build up period is desirable. The CMG described in reference [2] was allowed two hours to reach operating speed; yet the power required for this acceleration was twenty times that needed for constant speed operation.

Energy required for both torque motors is, using Eqs. (17) and (19):

$$E = 2\int_1^2 (I\ddot{\theta} + \omega_x H_R \cos\theta)\dot{\theta}\,dt = I(\dot{\theta}_2^2 - \dot{\theta}_1^2) + \int_1^2 T_c \omega_x\,dt \tag{20}$$

The maximum angular impulse absorbed, assuming the wheel spin axes are initially aligned with the spin reference axis, is, using Eq. (17):

$$A_{max} = 2H_R \int \dot{\theta}\cos\theta\,dt = 2H_R \sin\theta_{max} \tag{21}$$

A twin controller for each vehicle principal axis would be necessary for complete attitude control.

A two DOF CMG is shown in Fig. 7; the wheel drive motor is not visible. An additional torquer and gimbal freedom enable this CMG to produce gyroscopic control torque about two perpendicular axes. The

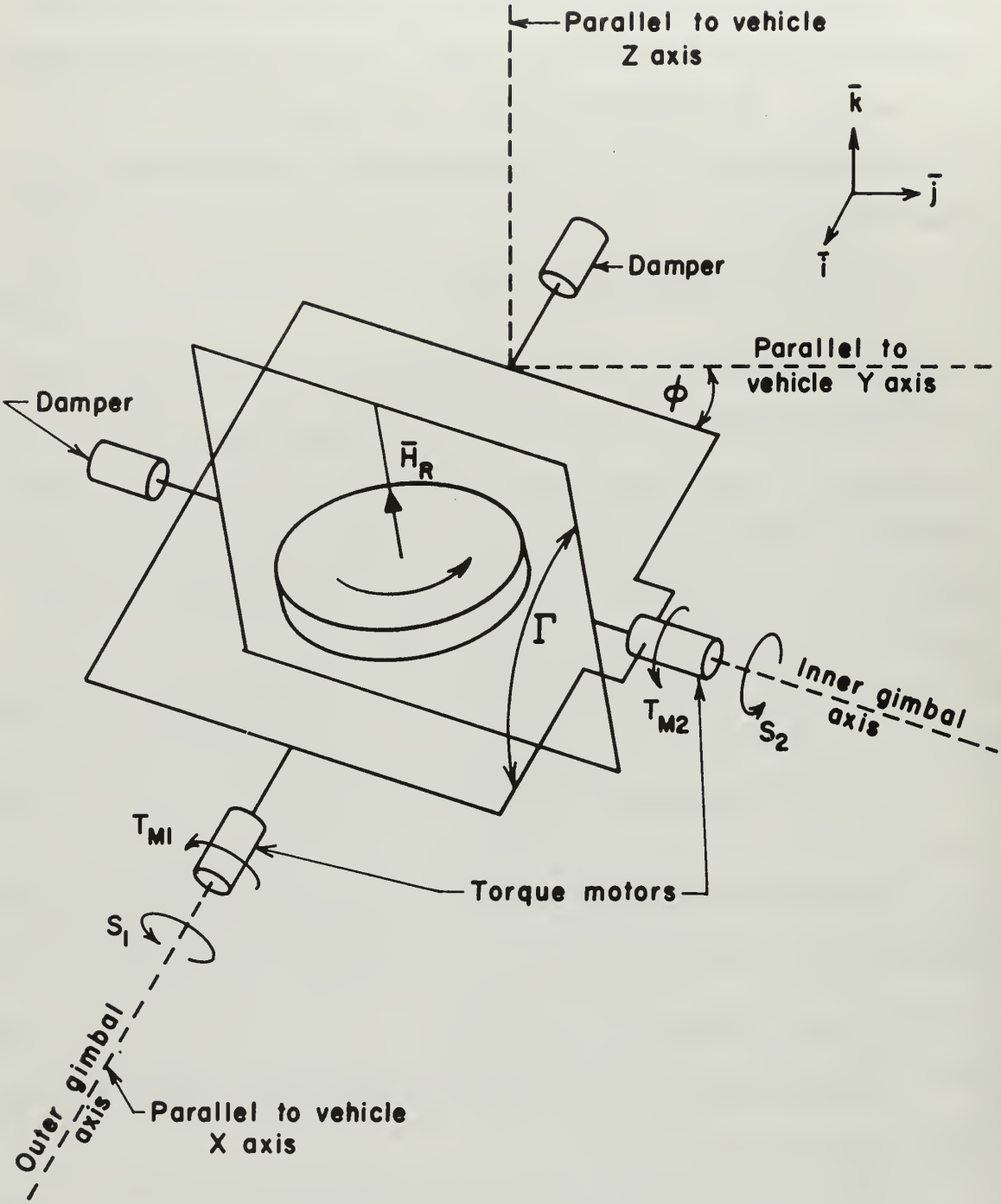

Figure 7

Two Degree of Freedom Control Moment Gyro

following discussion of the two DOF CMG utilizes the directions of angular motion arbitrarily assumed in Fig. 7. As with the single DOF CMG, control torque is effected by precessing wheel angular momentum. However, with this device the gyroscopic torque is transmitted primarily through the torque motors; the single DOF CMG control torque was conveyed to the vehicle by the gimbals and their supports. For example, control torque about the x axis is obtained by the inner gimbal axis torque motor rotating the inner gimbal. The resulting gyroscopic torque is $S_2 H_R$; the component about the x axis is $S_2 H_R \sin \Gamma$ and is transmitted to the vehicle via the outer gimbal axis torque motor. The component $S_2 H_R \cos \Gamma$ is perpendicular to the two gimbal axes and is the only control torque not conveyed to the vehicle by a torque motor. Rotation of the outer gimbal by its torque motor causes a torque, $S_1 H_R \sin \Gamma$, that is totally about the inner gimbal axis and must be transmitted to the vehicle by the inner gimbal axis torque motor. In referring to torque motor induced gimbal rotation, the assumption is made that $S_1 \simeq \dot{\phi}$ and $S_2 \simeq \dot{\Gamma}$.

The interdependency of the two torquers and gimbal rotations is evident in the gimbal equations of motion.

$$\left.\begin{aligned} T_{M_1} - D\dot{\phi} + S_2 H_R \, SIN\Gamma &= I_1 \dot{S}_1 \\ T_{M_2} - D\dot{\Gamma} - S_1 H_R \, SIN\Gamma &= I_2 \dot{S}_2 \end{aligned}\right\} \qquad (22)$$

where I_1 and I_2 are gimbal plus wheel moments of inertia about the outer and inner axes, respectively; I_2 is constant and I_1 varies with Γ. Equation (22) shows that as Γ departs from 90°, the gyroscopic torques diminish. When ϕ differs from zero, the torque about the inner gimbal axis is no longer parallel to the vehicle y axis. Both of these developments are undesirable and indicate a need for gimbal limits; reference

[6] suggests Γ and ϕ both be limited to one radian deflection from their initial displacements of $\Gamma = 90^\circ$ and $\phi = 0^\circ$. Remembering that the motor torque, as shown, is acting on the gimbals, the control torque on the vehicle is:

$$\bar{T}_c = -T_{M_1}\bar{i} + (S_2 H_R \cos\Gamma \sin\phi - T_{M_2}\cos\phi)\bar{j} + (S_2 H_R \cos\Gamma \cos\phi + T_{M_2}\sin\phi)\bar{k} \tag{23}$$

Combining Eqs. (22) and (23) yields:

$$\begin{aligned}\bar{T}_c = {} & \left[-D\dot{\phi} + S_2 H_R \sin\Gamma - I_1 \dot{S}_1\right]\bar{i} \\ & + \left[S_2 H_R \cos\Gamma \sin\phi - (D\dot{\Gamma} + S_1 H_R \sin\Gamma + I_2 \dot{S}_2)\cos\phi\right]\bar{j} \\ & + \left[S_2 H_R \cos\Gamma \cos\phi + (D\dot{\Gamma} + S_1 H_R \sin\Gamma + I_2 \dot{S}_2)\sin\phi\right]\bar{k}\end{aligned} \tag{24}$$

An order of magnitude analysis of Eq. (24) permits the dropping of the damping terms $D\dot{\phi}$ and $D\dot{\Gamma}$. If the suggested gimbal limits are observed, the term $S_2 H_R \cos\Gamma \sin\phi$ is negligible. These considerations result in:

$$\begin{aligned}\bar{T}_c \simeq {} & \left[S_2 H_R \sin\Gamma - I_1 \dot{S}_1\right]\bar{i} \\ & - \left[(S_1 H_R \sin\Gamma + I_2 \dot{S}_2)\cos\phi\right]\bar{j} \\ & + \left[S_2 H_R \cos\Gamma \cos\phi + (S_1 H_R \sin\Gamma + I_2 \dot{S}_2)\sin\phi\right]\bar{k}\end{aligned} \tag{25}$$

where the gyroscopic terms $S_2 H_R \sin\Gamma$ and $S_1 H_R \sin\Gamma \cos\phi$ predominate.

Determination of the angular impulse capacity of the two DOF CMG is facilitated by considering the components of the absolute gimbal rates, S_1 and S_2.

$$\begin{aligned}S_1 &= \dot{\phi} + \omega_x \\ S_2 &= \dot{\Gamma} + \omega_y \cos\phi + \omega_z \sin\phi\end{aligned}, \tag{26}$$

where ω_y and ω_z have the proper algebraic sign. Since control torque exists primarily about the vehicle x and y axes, the impulse about only these axes is computed. Saturation of the two DOF CMG occurs when Γ_{min} and ϕ_{max} are reached. If the gimbals are initially at $\Gamma = 90^{o}$ and $\phi = 0^{o}$, the maximum angular impulses accumulated about the x and y axes are, using Eqs. (25) and (26):

$$A_{x_{max}} = \int (S_2 H_R \sin\Gamma - I_1 \dot{S}_1)\, dt = -H_R \cos\Gamma_{min} + H_R \int (\omega_y \cos\phi + \omega_z \sin\phi) \sin\Gamma\, dt$$
$$- \int I_1 (\ddot{\phi} + \dot{\omega}_x)\, dt \qquad (27)$$

$$A_{y_{max}} = -\int (S_1 H_R \sin\Gamma + I_2 \dot{S}_2) \cos\phi\, dt = -H_R \int \dot{\phi} \sin\Gamma \cos\phi\, dt$$
$$- H_R \int \omega_x \sin\Gamma \cos\phi\, dt$$
$$- I_2 \int (\ddot{\Gamma} + \dot{\omega}_y \cos\phi - \omega_y \dot{\phi} \sin\phi + \dot{\omega}_z \sin\phi + \omega_z \dot{\phi} \cos\phi) \cos\phi\, dt \qquad (28)$$

A look at the relative magnitudes of the factors comprising Eqs. (27) and (28) leads to reduction in terms. H_R is by far the largest number; I_1, I_2, $\dot{\omega}_x$ and $\dot{\omega}_y$ are small numbers. The term $-H_R \int \dot{\phi} \sin\Gamma \cos\phi\, dt$ in Eq. (28) is unintegrable in present form; for illustration purposes an average Γ is assumed. Equations (27) and (28) can now be approximated by:

$$A_{x_{max}} \simeq -H_R \cos\Gamma_{min} + H_R \int (\omega_y \cos\phi + \omega_z \sin\phi) \sin\Gamma\, dt \qquad (29)$$

$$A_{y_{max}} \simeq -H_R \sin\phi_{max} \sin\Gamma_{average} - H_R \int \omega_x \sin\Gamma \cos\phi\, dt \;, \qquad (30)$$

where the first term on the right side of each equation usually predominates.

A twin two DOF CMG configuration similar to Fig. 6 provides similar cancelling of unwanted torques. Figure 8 is a schematic of such a device showing only the torque motors, momentum vectors and appropriate axes.

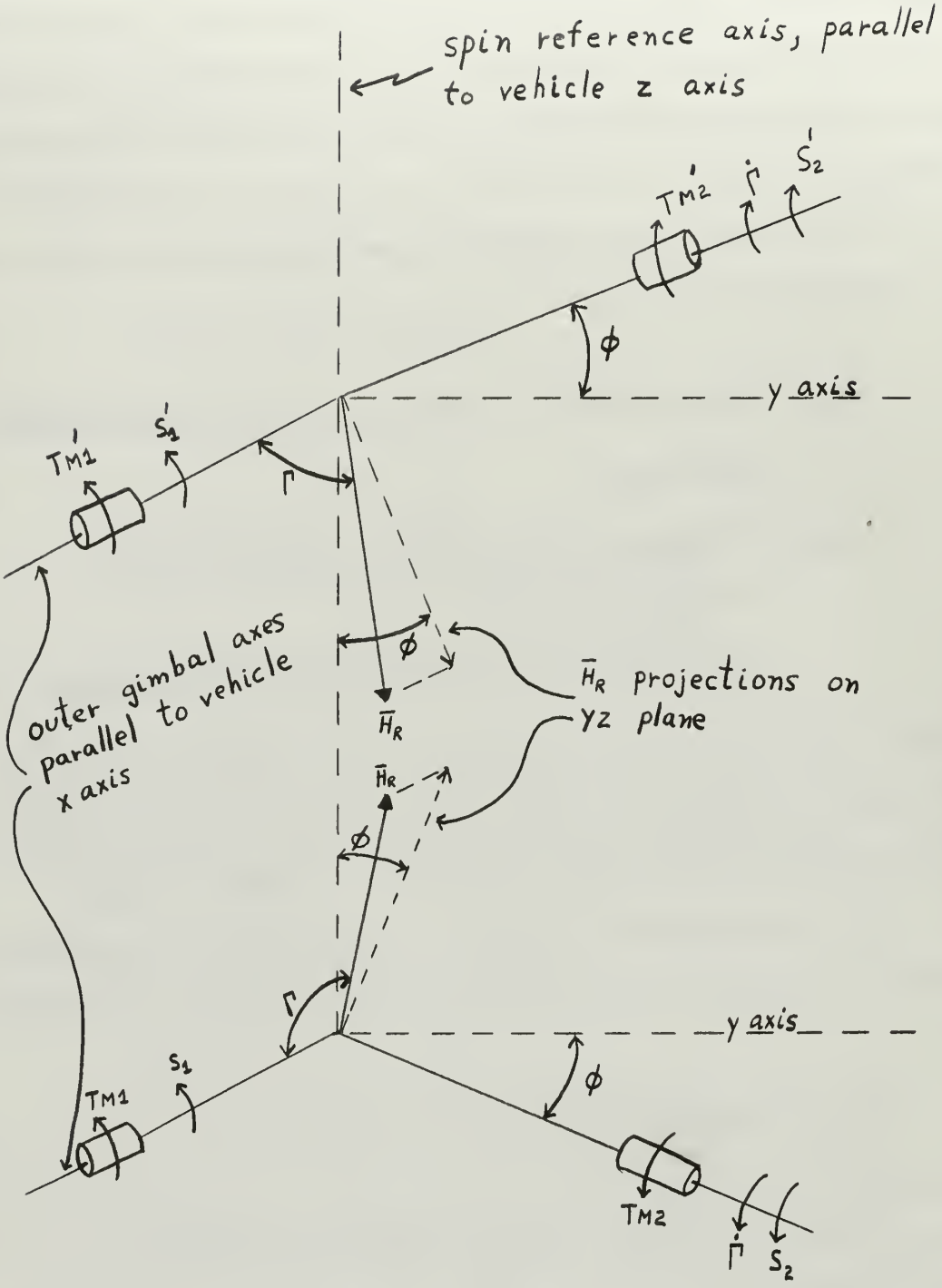

Figure 8

Twin Two Degree of Freedom Control Moment Gyro

As with the twin single DOF CMG, the deflections of the wheel spin axes from the spin reference axis are mirror images. The directions of torque and angular motion shown in Fig. 8 are for control torque about the vehicle x axis. As with the previous twin CMG, it is convenient to examine separately the gyroscopic torque caused by vehicle angular velocity and gimbal angular motion relative to the vehicle. The following analysis applies to Fig. 8; the primed quantities denote the properties of the upper wheel.

$$\bar{H}_R = H_R\left[\cos\Gamma\,\bar{i} + \sin\Gamma\sin\phi\,\bar{j} + \sin\Gamma\cos\phi\,\bar{k}\right]$$

$$\bar{H}_R' = H_R\left[\cos\Gamma\,\bar{i} + \sin\Gamma\sin\phi\,\bar{j} - \sin\Gamma\cos\phi\,\bar{k}\right]$$

$$\text{Net } \bar{H}_R = 2H_R\left[\cos\Gamma\,\bar{i} + \sin\Gamma\sin\phi\,\bar{j}\right] \tag{31}$$

$$\dot{\bar{\Gamma}} = \dot{\Gamma}\left[\cos\phi\,\bar{j} - \sin\phi\,\bar{k}\right]$$

$$\dot{\bar{\Gamma}}' = -\dot{\Gamma}\left[\cos\phi\,\bar{j} + \sin\phi\,\bar{k}\right]$$

$$\dot{\bar{\Gamma}}\times\bar{H}_R + \dot{\bar{\Gamma}}'\times\bar{H}_R' = 2H_R\dot{\Gamma}\left[\sin\Gamma\,\bar{i} - \cos\Gamma\sin\phi\,\bar{j}\right] \tag{32}$$

Equation (32) describes the net gyroscopic control torque produced by rotation of the inner gimbals by the inner gimbal axes torque motors. If Γ and ϕ are each limited to one radian deflection, $\sin\Gamma \gg \cos\Gamma\sin\phi$, and the y axis component in Eq. (32) is negligible. The torque components of the inner gimbal torque motors about the y axis cancel; the components about the z axis are additive and together equal $2\,T_{M2}\sin\phi$. Presumably control torque from a single controller would be generated about one axis at a time. Thus, for the case of control torque about the x axis, $\dot{\phi} = 0$, and T_{M2} is effecting $\dot{\Gamma}$ and not transferring appreciable gyroscopic torque to the vehicle. Since T_{M2} and $\sin\phi$ are both small, the z axis component is negligible.

A similar analysis for control torque about the y axis is accomplished by reversing the direction of the upper x axis motor torque. The resulting gyroscopic control torque is:

$$\bar{\dot{\phi}} \times \bar{H}_R + \bar{\dot{\phi}}' \times \bar{H}_R' = -2H_R \dot{\phi} \sin\Gamma \cos\phi \, \bar{J} \tag{33}$$

In general, unwanted gyroscopic torque will be caused by vehicle angular velocity precession of the net controller momentum. The twin configuration and gimbal limits serve to reduce the net momentum and therefore the unwanted torque.

Neglecting damping torques and gimbal accelerations, the angular impulse capacities about the x and y axes are, using Eqs. (32) and (33):

$$A_{x_{max}} = 2\int T_{M1}\, dt \simeq 2H_R \int \dot{\Gamma} \sin\Gamma \, dt = -2H_R \cos\Gamma_{min} \tag{34}$$

$$A_{y_{max}} = 2\int T_{M2} \cos\phi \, dt \simeq -2H_R \int \dot{\phi} \sin\Gamma \cos\phi \, dt$$

$$= -2H_R \sin\Gamma_{average} \sin\phi_{max} \, , \tag{35}$$

where, again for purposes of illustration, in Eq. (35) an average Γ has been assumed. As expected, Eqs. (34) and (35) show essentially double the angular impulse capacities of the single wheels described by Eqs. (29) and (30).

Torque motor power, less motor losses, for the case of control torque about the x axis, where $\dot{\phi} = 0$, is:

$$P_x = \dot{\Gamma}(T_{M2} + T_{M2}') \tag{36}$$

For the directions assumed in Fig. 8, the following holds:

$$T_{M2} = I_2 \dot{S}_2 + S_1 H_R \sin\Gamma$$

$$T_{M2}' = I_2 \dot{S}_2' + S_1' H_R \sin\Gamma \tag{22}$$

$$S_1 = \dot{\phi} + \omega_x = \omega_x = S_1'$$

$$S_2 = \dot{\Gamma} + \omega_y \cos\phi - \omega_z \sin\phi$$

$$S_2' = \dot{\Gamma} - \omega_y \cos\phi - \omega_z \sin\phi$$

$$\dot{S}_2 = \ddot{\Gamma} + \dot{\omega}_y \cos\phi - \dot{\omega}_z \sin\phi$$

$$\dot{S}_2' = \ddot{\Gamma} - \dot{\omega}_y \cos\phi - \dot{\omega}_z \sin\phi$$

Using these relationships Eq. (36) becomes:

$$P_x = 2\dot{\Gamma}\left[I_2(\ddot{\Gamma} - \dot{\omega}_2 \sin\phi) + \omega_x H_R \sin\Gamma\right] \simeq 2\dot{\Gamma}\left[I_2\ddot{\Gamma} + \omega_x H_R \sin\Gamma\right] \quad , \tag{37}$$

where the term $-2\dot{\Gamma} I_2 \dot{\omega}_2 \sin\phi$ has been dropped because of the lesser order of magnitude of $\dot{\omega}_2 \sin\phi$. A similar analysis for the case of control torque about the y axis yields:

$$P_y = \dot{\phi}\left(T_{M1} + T_{M1}'\right) = 2\dot{\phi}\left[I_1\ddot{\phi} + \omega_y H_R \cos\phi \sin\Gamma\right] \tag{38}$$

Torque motor energy, less motor losses, for control about the x axis is, using Eqs. (32) and (37):

$$E_x = 2I_2\int_1^2 \dot{\Gamma}\ddot{\Gamma}\,dt + \int_1^2 2\dot{\Gamma}\omega_x H_R \sin\Gamma\,dt = I_2\left(\dot{\Gamma}_2^2 - \dot{\Gamma}_1^2\right) + \int_1^2 T_x \omega_x\,dt \tag{39}$$

Similarly, for control about the y axis the torque motor energy is:

$$E_y = I_1\left(\dot{\phi}_2^2 - \dot{\phi}_1^2\right) + \int_1^2 T_y \omega_y\,dt \tag{40}$$

Three twin two DOF CMG could be arranged to provide control torque from two controllers about each vehicle principal axis.

Momentum dumping. The term, momentum dumping, refers to the removal of accumulated angular impulse from ME ACS. For the reaction wheel or

sphere it is a matter of decelerating the rotating element; for any of the CMG discussed it involves aligning the wheel spin axes with the spin reference axis. Saturation is caused by long acting unidirectional disturbance torque such as may result from solar pressure, meteorites or gas leakage. Presumably any ME ACS would be designed with sufficient impulse capacity to handle all attitude commands and oscillatory disturbances. Dumping may be effected by solar pressure or jet reaction torque. Since solar torque is very small, it would necessarily be a continuous acting system that would prevent the ME ACS from reaching saturation.

Jet reaction appears the more likely candidate; it is more reliable and easier to mechanize. With jet reaction dumping there is a trade off between A_{max} of the ME device and the fuel required for the reaction jets; as A_{max} is increased, the frequency of dumping decreases. Since A_{max} is proportional to $H_R = I_R \Omega$ for all ME ACS, increase in A_{max} will require additional weight in the form of a larger wheel or bigger drive motor to maintain higher Ω .

SECTION IV

COMPARISON OF ACS

The following is a discussion of the relative merits of three of the ME ACS. Reaction sphere and solar torque ACS are excluded. The reaction sphere is omitted because it has yet to prove feasible. Its theoretical advantage is that it accomplishes with a single rotating element that which requires three of either of the other type of ME ACS. In addition to suspension and torquing difficulties, disadvantages of the reaction sphere are: The required torquing power is comparable to that of the reaction wheel and therefore suffers the same disadvantage that is noted in the next section; momentary power interruption for a magnetically or electrostatically suspended sphere results in total failure. Solar torque is not compared since, with the control surface sizes presently deemed practical, it is insufficient for commanded attitude changes.

Bases for comparison are: power and energy, weight, angular impulse capacity, pointing accuracy, reliability, size and cost. Sizes of the ME ACS are not compared since, with the exception of the reaction sphere, they do not vary appreciably. Cost is also not considered.

The comparisons, in general, are not numerical; such comparison would require numerical evaluation of the weights, efficiencies and reliabilities of the torque and drive motors. The ACS compared are the reaction wheel, twin single DOF CMG and twin two DOF CMG. It is assumed that the superior performance of the twin configurations compared to the single CMG controllers would discourage the selection of the latter. Each ACS is assumed to consist of three controllers oriented parallel to vehicle principal axes. The applicable equations are listed in Fig. 9 for ease of reference.

Individual Controllers

		control torque	net angular momentum	maximum angular impulse	power	energy
reaction wheel		(10) $I_R(\dot{\Omega}-\dot{\omega}_x)$	$I_R(\Omega \pm \omega_x)$	(15) $I_R \Omega_{max}$	(13) $I_R(\dot{\Omega}-\dot{\omega}_x)\Omega$	(14) $\frac{I_R}{2}\left[(\Omega_2-\omega_{x_2})^2-(\Omega_1-\omega_{x_1})^2\right] + \int_1^2 T_x \omega_x dt$
twin single DOF CMG		(17) $2H_R \dot{\theta} \cos\theta$	$2H_R \sin\theta$	(21) $2H_R \sin\theta_{max}$	(19) $2\dot{\theta}\left[I\ddot{\theta}+H_R\omega_x\cos\theta\right]$ + 2 drive motors	(20) $I(\dot{\theta}_2^2-\dot{\theta}_1^2) + \int_1^2 T_x\omega_x dt$ + 2 drive motors
twin two DOF CMG	x comp	(32) $2H_R \dot{\Gamma} \sin\Gamma$	$2H_R \cos\Gamma$	(34) $2H_R \cos\Gamma_{min}$	(37) $2\dot{\Gamma}\left[I_2\ddot{\Gamma}+H_R\omega_x\sin\Gamma\right]$ + 2 drive motors	(39) $I_2(\dot{\Gamma}_2^2-\dot{\Gamma}_1^2) + \int_1^2 T_x\omega_x dt$ + 2 drive motors
	y comp	(33) $2H_R \dot{\phi} \sin\Gamma\cos\phi$	$2H_R \sin\Gamma\cos\phi$	(35) $2H_R \sin\Gamma_{ave}\cos\phi_{max}$	(38) $2\dot{\phi}\left[I_1\ddot{\phi}+H_R\omega_y\sin\Gamma\cos\phi\right]$ + 2 drive motors	(40) $I_1(\dot{\phi}_2^2-\dot{\phi}_1^2) + \int_1^2 T_y\omega_y dt$ + 2 drive motors

Figure 9

Summary of Equations

Power and energy comparison. In comparing ME ACS, power and energy need not be differentiated if, for a given control torque and vehicle angular velocity, the power is always the same; i.e., the power required for the ACS is independent of the state of the ACS. Reaction wheels violate this condition; power is proportional to Ω. The single and two DOF CMG behave identically in this respect; Eqs. (17) and (19) and the fact that the term, $2\dot{\theta}H_R\omega_x\cos\theta$, is predominant show that CMG power is essentially independent of gimbal position. Maximum power is a critical factor in spacecraft systems; the varying power of a reaction wheel system for identical dynamic response is undesirable.

It is illustrative to observe the fraction of total power that goes into torquing the vehicle; the remainder serves to accelerate ACS components. For the reaction wheel this fraction is, using Eqs. (12) and (13):

$$\frac{T_x\omega_x}{I_R(\dot{\Omega}-\dot{\omega}_x)\Omega} = \frac{\omega_x}{\Omega} \ll 1 \tag{41}$$

For the twin single DOF CMG, using Eqs. (17) and (19) and neglecting drive motor power, this fraction is:

$$\frac{T_x\omega_x}{2\dot{\theta}\left[I\ddot{\theta}+H_R\omega_x\cos\theta\right]} = \frac{H_R\omega_x\cos\theta}{I\ddot{\theta}+H_R\omega_x\cos\theta} \simeq 1 \tag{42}$$

since $I\ddot{\theta} \ll H_R\omega_x\cos\theta$. Similarly for the twin two DOF CMG the fractions for the x and y axes are, respectively:

$$\frac{H_R\omega_x \sin\Gamma}{I_2\ddot{\Gamma}+H_R\omega_x\sin\Gamma} \simeq 1$$

and

$$\frac{H_R\omega_y \sin\Gamma\cos\phi}{I_1\ddot{\phi}+H_R\omega_y\sin\Gamma\cos\phi} \simeq 1 \quad , \tag{43}$$

where again drive motor power has been neglected. This omission is justified if drive motor power is negligible compared to the power expended torquing the vehicle, the latter quantity being dependent on the required torque and the vehicle angular speed about the axis in question.

Drive motor power is minimized by using high quality bearings, carefully balancing wheels and surrounding the rotating element with a light gas at low pressure. The 50 ft-lb of control torque, two DOF CMG, described in reference [2] required 18 watts to maintain 12,000 rpm. A twin two DOF CMG producing 50 ft-lb would require 43 watts for torquer and drive motors if the vehicle were rotating at 0.1 rad/sec about the torque axis. A reaction wheel with a 100 per cent efficient drive motor, no windage and bearing losses, and equal wheel size and torque could not exceed 6 rpm if limited to 43 watts; and it would reach that speed in 0.01 seconds from rest.

The reaction wheel can compensate to a limited extent for its low efficiency by employing regenerative braking; i.e., when the direction of control torque and wheel speed are such as to require deceleration of the wheel, the drive motor can generate its own armature current down to a certain speed. Although some of the kinetic energy stored in the wheel is regained, the overall efficiency does not approach that of the CMG.

To summarize the power and energy comparison of the three ME ACS:

1. The single and two DOF CMG have identical energy conversion efficiencies.

2. As evidenced by Eqs. (14), (20), (39) and (40) and the power fractions, the major part of the energy input to a reaction wheel goes into changing the kinetic energy of the wheel; the only appreciable

energy loss in a CMG, outside of initial speed buildup, is motor, bearing and windage loss of the drive motor.

3. The reaction wheel is competitive, from a power and energy standpoint, when either infrequent use or small torque and low angular impulse capacity are needed. The latter condition results from power and A_{max} dependency on Ω as described by Eqs. (13) and (15), respectively. The first consideration reflects the constant drive motor power required for the CMG; a reaction wheel, when not in use, idles at a lower speed than an equivalent CMG, thereby requiring less power during such periods. This advantage can be negated somewhat by the following: With regard to the twin single DOF CMG shown in Fig. 6, the spin reference axis of an individual controller can be arbitrarily oriented in a plane perpendicular to the output axis without affecting the net angular momentum or the control torque. Figure 10 represents three identical twin controllers with spin axes aligned along their respective spin reference axes. Vectors $\bar{A}$, $\bar{B}$, $\bar{C}$, $\bar{A}'$, $\bar{B}'$ and $\bar{C}'$ represent the angular momentum vectors of the six wheels. The output axes of the three controllers are parallel to vehicle principal axes. Since the angular momenta of the six wheels are equal in magnitude, the particular orientation of Fig. 10 yields: $\bar{A}+\bar{B}+\bar{C} = 0$ and $\bar{A}'+\bar{B}'+\bar{C}' = 0$. If $\bar{A}$, $\bar{B}$ and $\bar{C}$ or $\bar{A}'$, $\bar{B}'$ and $\bar{C}'$ are aligned with their respective spin axes as shown and are brought to zero magnitude at equal rates, there is no net torque on the vehicle and the net momentum of the controllers remains zero. This procedure halves drive motor power. The reduced capability would normally be adequate for countering environmental disturbance torque. The preceding arrangement is applicable to the twin two DOF CMG as well.

x, y and z axes are torque output axes and are parallel to vehicle principal axes

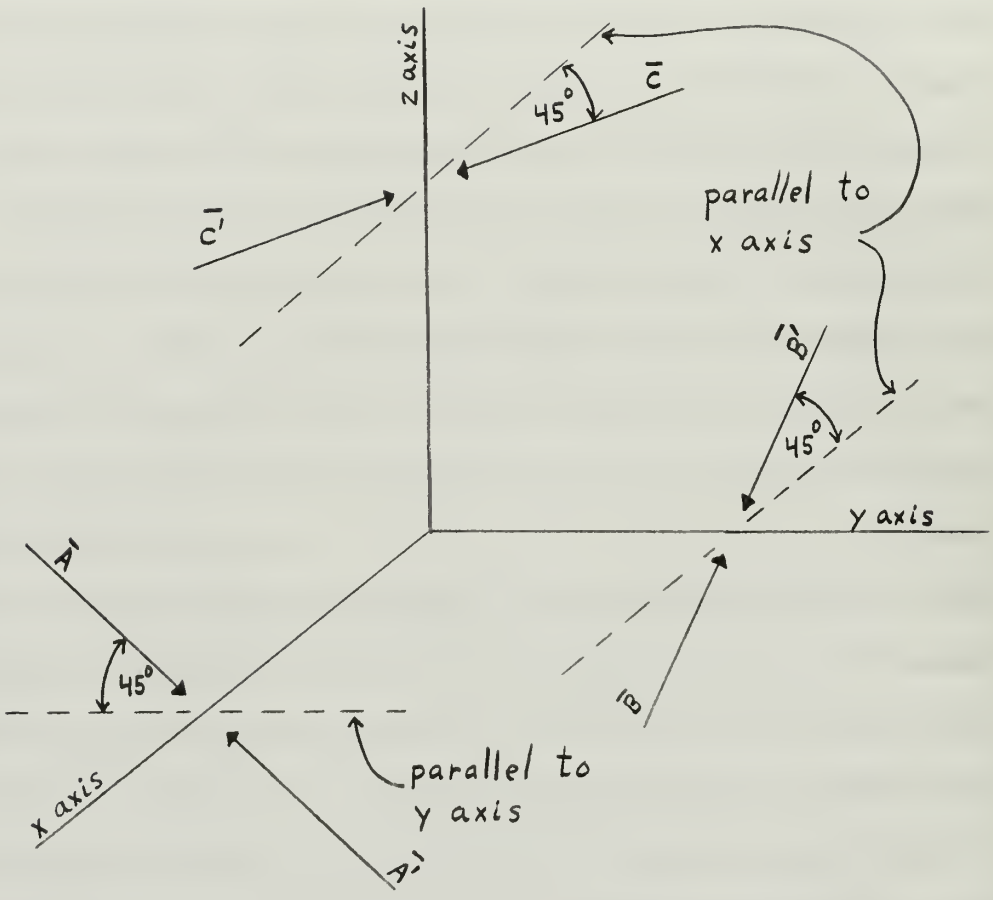

Figure 10

Three Twin Control Moment Gyros

Weight comparison. The rotating elements, torque motors and drive motors are the primary components contributing to the weight of ME ACS. As noted earlier, reaction wheels require larger I_R than do CMG, for the same torque and power; the larger I_R, of course, means increased weight. This difference is offset to a varying degree by the gimbals and extra motors required for CMG. Thus, from a weight comparison standpoint, the reaction wheel improves with decreasing control torque and becomes competitive when the larger weight of the wheel is offset by the weight of the gimbals and additional motors of the CMG.

The two types of CMG compare in much the same fashion as CMG in general compare with reaction wheels. With an ACS composed of three twin two DOF CMG, each axis can be torqued by two controllers. Therefore, an ACS consisting of three twin two DOF CMG requires half as much angular momentum per wheel as a similar system of single DOF CMG; this allows a wheel weight saving for the two DOF system. Although single and two DOF CMG require the same power, the latter lacks the torque multiplication of the single DOF CMG. The gearing necessary to achieve the higher torque results in extra weight for the two DOF system. Thus the two DOF CMG system is lighter than the single DOF system when the wheel weight saving offsets the additional weight of the gearing and the extra gimbal and torque motor. This situation arises with larger vehicles which require greater H_R for larger torques and angular impulse capacities.

Angular impulse capacity comparison. The angular impulse capacity of a reaction wheel is equal to the maximum angular momentum of the wheel. The impulse capacity of a CMG would also equal the H_R of the device were it not for gimbal limits imposed. This better "efficiency"

of the reaction wheel is more than offset by its typically low $H_{R\,max}$, which is a result of power considerations; from a power standpoint the reaction wheel cannot be torqued at the speeds of a comparable CMG.

A significant advantage of the two DOF CMG is the fact that its angular impulse capacity is nearly double that of the single DOF CMG.

Pointing accuracy comparison. As noted earlier, net momentum affords gyroscopic rigidity, thereby improving pointing accuracy. The variable net momentum of a reaction wheel system is comparable to that of either twin CMG system; the individual wheel momenta of the CMG are much greater than those of the reaction wheels, but a large percentage of the CMG momenta is cancelled by the twin configuration. The two types of CMG have identical pointing accuracy. CMG and reaction wheels are subject to similar electromechanical lag in the controllers.

In summary, there is no significant inherent difference in pointing accuracy capability between the three ACS.

Reliability comparison. The three ME ACS have in common the potentially dangerous situation of a rapidly spinning mass supported with a minimum of physical contact for extended time periods. Since actual hardware is not being evaluated, the relative reliability of the ACS may be discussed only in general terms. The reaction wheel, single DOF CMG and two DOF CMG increase in complexity in the order listed. The CMG differ only in the extra gimbal and torquer of the two DOF CMG. Since the motors and bearings of ME ACS are likely failure areas, the additional torquer of the two DOF CMG is a significant disadvantage. The constant and higher speeds of CMG make bearing failure more likely with them than with reaction wheels. The twin CMG configuration affords a limited amount of redundancy, providing failure of one wheel or

associated equipment does not incapacitate the other half of the controller. The twin two DOF CMG system provides further redundancy, in that control torque is available about all axes with one controller completely failed. The varying complexity of the three ME devices also appears in the gathering of control logic information from the controllers. With the reaction wheel, wheel speed is the only parameter monitored. For a single two DOF CMG, the control system must maintain constant wheel speed and monitor the angular motion of two gimbals.

Therefore, despite the ability of the CMG systems to function while partially failed, a rigorous reliability analysis of actual hardware would probably find the reliability varying inversely with the complexity; i.e., the reaction wheel is the most reliable and the two DOF CMG is the least reliable.

SECTION V

CONCLUSIONS

The observations made in Sec. IV lead to the following conclusions:

1. Solar pressure torque is insufficient for attitude control but may be utilized to prevent the saturation of ME ACS.

2. Reaction spheres have theoretical advantages, but there are mechanization problems still to be solved.

3. If power is critical and response time limited, reaction wheels must be relegated to relatively small vehicles; for larger vehicles the torque needed to achieve reasonable response time requires prohibitive power from a reaction wheel ACS.

4. For still larger vehicles the two DOF CMG has significant weight and angular impulse capacity advantages, but, with its increased complexity, it is the least reliable of the three ME ACS compared.

5. Selection of a mass conservative ACS, assuming cost is not pertinent, therefore hinges on vehicle size, required reliability and the relative priorities placed on ACS weight, power and angular impulse capacity.

BIBLIOGRAPHY

1. Lopez, A. E., and J. W. Ratcliff. Simulator Study of Precise Attitude Stabilization of a Manned Spacecraft by Twin Gyros and Pulse Modulated Reaction Jets. Ames Research Center. NASA TND-1645, 1964.

2. Yarber, G. W., K. T. Chang, J. Kukel, B. F. McKee, C. S. Smith, A. F. Anderson, C. J. Bertrem and S. Tarhov. Control Moment Gyro Optimization Study. Garrett Airesearch Manufacturing Division. NASA CR-400, 1966.

3. Wheeler, P. C., R. G. Nishinaga, J. G. Zaremba and H. L. Williams. Evaluation of a Semi Active Gravity Gradient System. TRW Systems. NASA CR-594, 1966.

4. Hering, K. W., and R. E. Hufnagel. "Inertial Sphere System for Complete Attitude Control of Earth Satellites," American Rocket Society Journal, XXXI (August, 1961), pp. 1074-1078.

5. Ormsby, R. D., and M. H. Smith. "Capabilities and Limitations of Reaction Spheres for Attitude Control," American Rocket Society Journal, XXXI (June, 1961), pp. 808-812.

6. Dohogne, J. R., and R. F. Morrison. "The Control Moment Gyroscope," Sperry Engineering Review (Spring, 1965), pp. 33-40.

7. Casaday, W. M. Reaction Wheel with Brushless D. C. Motor Drive. Sperry Farragut Company. NASA CR-388, 1966.

8. Bell, M. W. J. "An Evolutionary Program for Manned Interplanetary Explorations," Journal of Spacecraft and Rockets, IV (May, 1967), pp. 625-630.

9. Purser, P. E., M. A. Faget and N. F. Smith. Manned Spacecraft: Engineering and Design. New York: Fairchild Publications Inc., 1964.

10. Merrick, V. K., and F. J. Moran. The Highly Coupled System - A General Approach to the Passive Attitude Stabilization of Space Vehicles. Ames Research Center. NASA TND-3480, 1966.

11. Roberson, R. E. "Torques on a Satellite Vehicle from Internal Moving Parts," Journal of Applied Mechanics, XXV (June, 1958), pp. 196-200.

12. Cannon, R. H. "Gyroscopic Coupling in Space Vehicle Attitude Control Systems," Journal of Basic Engineering, LXXXIV (March, 1962), p. 81.

13. Jacot, A. D., and D. J. Liska. "Control Moment Gyros in Attitude Control," Journal of Spacecraft and Rockets, III (September, 1966), pp. 1313-1320.

APPENDIX A

GRAVITY GRADIENT TORQUE

The important aspects of gravity gradient torque are illustrated by a model consisting of two spheres of equal mass connected by a massless rod and subject to an inverse square gravitational field.

Notation:

$m_1 = m_2 = m$ = mass of rod connected spheres

M = mass of attracting body

G = universal gravitational constant

T = gravity induced torque

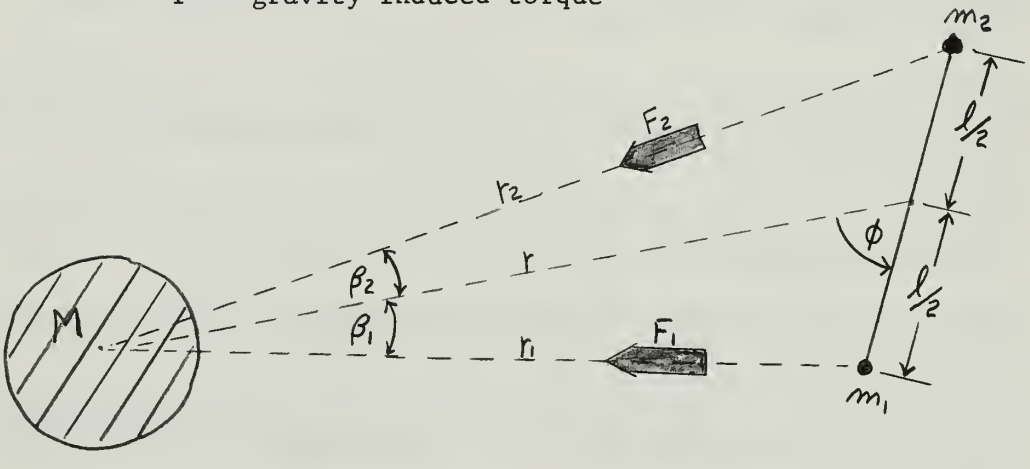

Newton's law: $F_1 = \frac{GMm}{r_1^2}$, $F_2 = \frac{GMm}{r_2^2}$

$$T = \frac{\ell}{2}\left[F_2 \sin(\phi-\beta_2) - F_1 \sin(\phi+\beta_1)\right]$$

$$\frac{r}{\sin(\phi-\beta_2)} = \frac{r_2}{\sin\phi} \quad , \quad \frac{r}{\sin(\phi+\beta_1)} = \frac{r_1}{\sin\phi}$$

$$T = \frac{\ell}{2}\left[\frac{F_2 r \sin\phi}{r_2} - \frac{F_1 r \sin\phi}{r_1}\right] = \frac{1}{2} GMm\ell r \sin\phi \left[\frac{1}{r_2^3} - \frac{1}{r_1^3}\right]$$

The gravity gradient torque is zero when ϕ is zero. For any other orientation, except for the unstable $\phi = 90^o$ position, a torque exists.

This example may be generalized for an arbitrary body as follows. A body subject to an inverse square gravitational attraction experiences a torque tending to align its axis of minimum moment of inertia with the gravitational field.

APPENDIX B

EQUATIONS OF ANGULAR MOTION

Symbols used only in this appendix:

m_i = mass of i'th particle

$\bar{\rho}_i$ = position vector from system center of mass to i'th particle

The reference coordinate system is Cartesian with origin at the system center of mass and axes colinear with system principal axes. The system is assumed rigid except for rotation of ACS devices.

$$\bar{\rho}_i = x_i \bar{i} + y_i \bar{j} + z_i \bar{k} \quad , \qquad \bar{\omega} = \omega_x \bar{i} + \omega_y \bar{j} + \omega_z \bar{k}$$

Definitions:

$$I_{xx} = \sum_i m_i (y_i^2 + z_i^2) \quad , \quad I_{yy} = \sum_i m_i (x_i^2 + z_i^2) \quad , \quad I_{zz} = \sum_i m_i (x_i^2 + y_i^2)$$

$$I_{xy} = I_{yx} = - \sum_i m_i x_i y_i$$

$$I_{xz} = I_{zx} = - \sum_i m_i x_i z_i$$

$$I_{yz} = I_{zy} = - \sum_i m_i y_i z_i$$

$$\bar{H} = \sum_i \bar{\rho}_i \times m_i \dot{\bar{\rho}}_i$$

Equation derivations:

$$\dot{\bar{\rho}}_i = \left[\frac{d\bar{\rho}_i}{dt}\right]_{\bar{\omega}=0} + \bar{\omega} \times \bar{\rho}_i = \bar{\omega} \times \bar{\rho}_i \qquad \text{for a rigid body}$$

$$\therefore \bar{H} = \sum_i m_i \bar{\rho}_i \times (\bar{\omega} \times \bar{\rho}_i)$$

$$\bar{H} = \sum_i m_i \left\{ \left[(y_i^2 + z_i^2)\omega_x - x_i y_i \omega_y - x_i z_i \omega_z \right] \bar{i} \right.$$

$$\left. + \left[-y_i x_i \omega_x + (x_i^2 + z_i^2)\omega_y - y_i z_i \omega_z \right] \bar{j} + \left[-z_i x_i \omega_x - z_i y_i \omega_y + (x_i^2 + y_i^2)\omega_z \right] \bar{k} \right\}$$

$$\bar{H} = I_{xx} \omega_x \bar{i} + I_{yy} \omega_y \bar{j} + I_{zz} \omega_z \bar{k} \qquad (1)$$

Newton's Second Law as applied to angular motion:

$$\bar{T} = \dot{\bar{H}} = \left[\frac{d\bar{H}}{dt}\right]_{\bar{\omega}=0} + \bar{\omega} \times \bar{H} \tag{2}$$

Combining Eqs. (1) and (2):

$$\bar{T} = \left[I_{xx}\dot{\omega}_x + (I_{zz} - I_{yy})\omega_y\omega_z\right]\bar{i}$$
$$+ \left[I_{yy}\dot{\omega}_y + (I_{xx} - I_{zz})\omega_x\omega_z\right]\bar{j}$$
$$+ \left[I_{zz}\dot{\omega}_z + (I_{yy} - I_{xx})\omega_x\omega_y\right]\bar{k} \tag{3}$$

Equations for system composed of vehicle and ME ACS.

$$\bar{T}_E = \dot{\bar{H}} = \dot{\bar{H}}_v + \dot{\bar{H}}_R \ , \tag{4}$$

where $\bar{T}_E$ is torque external to the system as opposed to internal torque generated by interaction of system components. $\bar{H}_v$ and $\bar{H}_R$ are the angular momenta of the vehicle and wheel, respectively. In the absence of external torque:

$$\bar{H} = \bar{H}_v + \bar{H}_R = \text{CONSTANT}$$
$$\dot{\bar{H}} = \dot{\bar{H}}_v + \dot{\bar{H}}_R = 0$$
$$\bar{T}_c = \dot{\bar{H}}_v = -\dot{\bar{H}}_R \tag{5}$$

where $\bar{T}_c$ is control torque on the vehicle generated by the ME ACS. Combining Eqs. (2) and (5):

$$\bar{T}_c = -\left[\frac{d\bar{H}_R}{dt}\right]_{\bar{S}=0} - \bar{S} \times \bar{H}_R \ , \tag{6}$$

where $\bar{S}$ is the absolute angular velocity of the ACS spin axis; $\bar{S}$ differs from $\bar{\omega}$ when the spin axis moves relative to the vehicle. Since I_R, the moment of inertia of the rotating element about its spin axis, is

typically much larger than the element's moment of inertia about its other two principal axes:

$$\bar{H}_R \simeq I_R(\bar{\Omega} + \bar{\omega}_R) \quad , \tag{7}$$

where $\bar{\omega}_R$ is the component of vehicle angular velocity about the spin axis of the ACS.

For a reaction wheel or reaction sphere, using Eqs. (6) and (7):

$$\bar{T}_c = -\left[\frac{d\bar{H}_R}{dt}\right]_{\bar{S}=0} = -I_R\left[\frac{d(\bar{\Omega} + \bar{\omega}_R)}{dt}\right]_{\bar{S}=0} \tag{8}$$

For a control moment gyro (CMG), $\Omega \gg \omega_R$; using Eqs. (6) and (7):

$$\bar{T}_c = -\bar{S} \times \bar{H}_R = -I_R(\bar{S} \times \bar{\Omega}) \tag{9}$$

APPENDIX C

BRUSHLESS D.C. MOTOR DRIVEN INERTIA WHEEL BUILT BY SPERRY FARRAGUT COMPANY FOR NASA.

General description. The motor is bidirectional. The entire unit is hermetically sealed. Conventional commutation is replaced by photo optical detectors and transistorized switches thus avoiding physical contact between commutator and armature. Energy saving regenerative braking is employed; voltage generated in armature windings affords complete control of wheel when decelerating. When the counter EMF decreases to where it can no longer produce required armature current, the system is automatically switched to a "driving mode."

Motor wheel characteristics.

Total weight	-	13.7 lb
Size	-	1 ft x 1 ft x ¼ ft
Power required	-	40 watts max
Control torque	-	0.65 ft-lb @ 0-250 rpm
Friction torque	-	0.023 ft-lb
H_R	-	1 ft-lb-sec @ 250 rpm
I_R	-	1.25 lb-ft^2
RPM	-	0-550

The contractor offered the following reliability prediction for the motor-wheel combination, considering all components in series and assuming any component failure to be a complete failure:

	RELIABILITY		
	1000 HRS	1 YR	3 YRS
Motor and wheel actually constructed:	98%	84%	59%
Identical device with high reliability parts:	99%	89%	71%

The preceding reliability estimate is based on the following power level operation: peak power 1 per cent of the time, half of peak power 5 per cent of the time and 6.9 per cent peak power 94 per cent of the time.

APPENDIX D

THEORETICAL, MAGNETICALLY SUSPENDED AND TORQUED REACTION SPHERE [4]

Spherical shell radius	9.8 in
Spherical shell thickness	.2 in
Spherical shell material	aluminum
Spherical shell weight	23.4 lb
Ω @ maximum T_c	54 rad/sec
Maximum torquing power	18 watts
Maximum T_c	.103 ft-lb
Torquing coils weight	66.2 lb
Effective suspension "spring constant"	5.72×10^{-3} lb/in
Suspension power	8.4 watts
Suspension coils weight	11.1 lb
Total weight excluding housing and electronics	101 lb
Total power	26.4 watts

INITIAL DISTRIBUTION LIST

		No. Copies
1.	Defense Documentation Center Cameron Station Alexandria, Virginia 22314	20
2.	Library Naval Postgraduate School Monterey, California 93940	2
3.	Commander, Naval Air Systems Command Department of the Navy Washington, D. C. 20360	1
4.	Chairman, Department of Aeronautics Naval Postgraduate School Monterey, California 93940	2
5.	Dr. Cameron M. Smith Department of Aeronautics Naval Postgraduate School Monterey, California 93940	1
6.	LT David S. Gilbreath, USN Route 1, Box 440J Oak Harbor, Washington	1
7.	Dr. Allen E. Fuhs Department of Aeronautics Naval Postgraduate School Monterey, California 93940	1

DOCUMENT CONTROL DATA · R&D

(Security classification of title, body of abstract and indexing annotation must be entered when the overall report is classified)

1. ORIGINATING ACTIVITY (Corporate author)	2a. REPORT SECURITY CLASSIFICATION
Naval Postgraduate School Monterey, California	UNCLASSIFIED
	2b. GROUP

3. REPORT TITLE

MASS CONSERVATIVE ATTITUDE CONTROL SYSTEMS FOR INTERPLANETARY SPACECRAFT

4. DESCRIPTIVE NOTES (Type of report and inclusive dates)

Thesis, M.S. in Aeronautical Engineering, Sept 1967

5. AUTHOR(S) (Last name, first name, initial)

GILBREATH, David S.

6. REPORT DATE	7a. TOTAL NO. OF PAGES	7b. NO. OF REFS
September 1967	58	13

8a. CONTRACT OR GRANT NO.	9a. ORIGINATOR'S REPORT NUMBER(S)
b. PROJECT NO.	
c.	9b. OTHER REPORT NO(S) (Any other numbers that may be assigned this report)
d.	

10. AVAILABILITY/LIMITATION NOTICES

[redacted]

11. SUPPLEMENTARY NOTES	12. SPONSORING MILITARY ACTIVITY
	Naval Air Systems Command

13. ABSTRACT

Attitude control requirements for interplanetary space are discussed. Spacecraft attitude control systems, excluding mass expulsion devices, are described. Solar pressure, reaction spheres, reaction wheels and control moment gyros are analyzed as sources of control torque. A comparison is made between the reaction wheel and two types of control moment gyros on the basis of weight, power consumption, momentum absorption capability and reliability. The control moment gyros are shown to be the most promising for larger vehicles.

DD FORM 1 JAN 64 1473

14. KEY WORDS	LINK A		LINK B		LINK C	
	ROLE	WT	ROLE	WT	ROLE	WT
Attitude control systems						
Control moment gyro						
Reaction wheel						